Supporting Information for

Submarine Morphological Description of the Ancient Archipelagic Aprons in the Marcus–Wake Seamount Group, Northwestern Pacific Ocean

Xiao Wang [1], Huaiming Li [1,2,*], Yongshou Cheng [3], Pengfei Yao [1], Fengyou Chu [1], Weilin Ma [1], Hongyi Wang [2], Shihui Lv [4], Xiaohu Li [1], Zhenggang Li [1], Weiyan Zhang [1] and Yanhui Dong [1]

[1] Key Laboratory of Submarine Geosciences, Second Institute of Oceanography, Ministry of Natural Resources, Hangzhou 310012, China; wangxiao@sio.org.cn (X.W.); yaopf@sio.org.cn (P.Y.); chu@sio.org.cn (F.C.); weilin_ma@sio.org.cn (W.M.); xhli@sio.org.cn (X.L.); lizg@sio.org.cn (Z.L.); zwy885@163.com (W.Z.); dongyh@sio.org.cn (Y.D.)
[2] Beijing Pioneer High-Tech Corporation, Beijing 100081, China; sallywang166@sina.com
[3] National Marine Data Information Center, Tianjin *300012*, China; yshcheng@163.com
[4] School of Ocean Sciences, China University of Geosciences (Beijing), Beijing 100083, China; lvshihui@cugb.edu.cn
* Correspondence: huaiming_lee@163.com

Contents of this file

Figure S1. (a–b) Topographic profile of the Suda guyot.

Figure S2. (a–b) Topographic profile of the Aronld guyot.

Figure S3. Sediment waves topography profile of Suda guyot.

Figure S4. Sediment waves topography profile of Arnold guyot.

Figure S5. Sediment waves topography profile of Lamont guyot.

Figure S6. Sediment waves topography profile of Niulang and Zhinyv guyot.

Figure S7. Relationship between the width and relief of gullies and channels.

Figure S8. Relationship between the width and slope of gullies and channels.

Figure S9. Relationship between the relief and slope of gullies and channels.

Figure S10. Relationship between the width and height of gullies and channels.

Figure S11. Relationship between the wavelength and slope of sediment waves at different scales.

Figure S12. Relationship between the wave height and slope of sediment waves at different scales.

Figure S13. Small-scale sediment wave formation model (modified from Symons et al., 2016) [22].

Table S1. Submarine fan topography data.

Table S2. Sediment waves topography data.

Introduction

The software of Global Mapper was used to estimate various geomorphic features following the methodology described in Gardner et al. (2021) [3] and Watt et al. (2014) [14]. The results of these analyses are presented in Table S1. In addition, cross-sectional profiles of the terrain were extracted at 5-km intervals between gullies and channels, and parameters such as width, relief, and slope on both sides were derived from the profiles. Following the methodology described in Symons et al. (2016) [22], Global Mapper was utilized to extract parameters such as wavelength, wave height, and slope of sediment waves deposit. The results of these analyses are presented in Table S2.

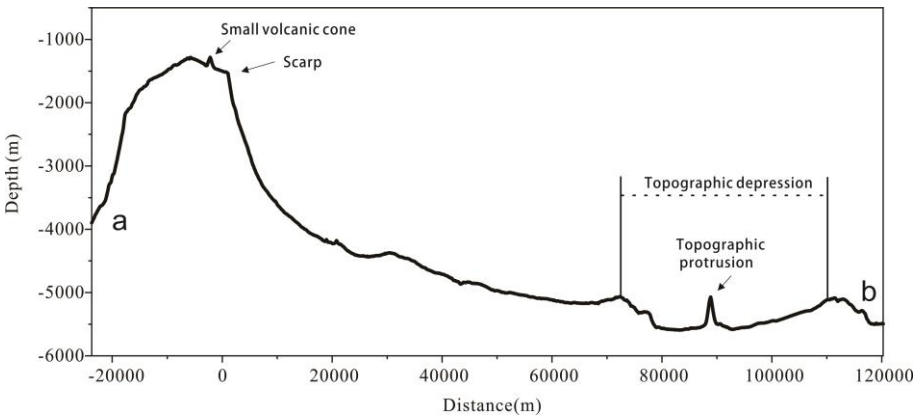

Figure S1. (a–b) Topographic profile of the Suda guyot.

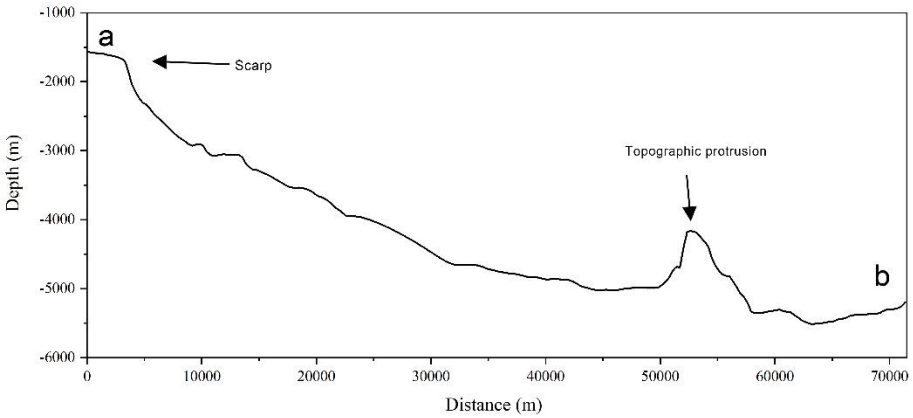

Figure S2. (a–b) Topographic profile of the Aronld guyot**.**

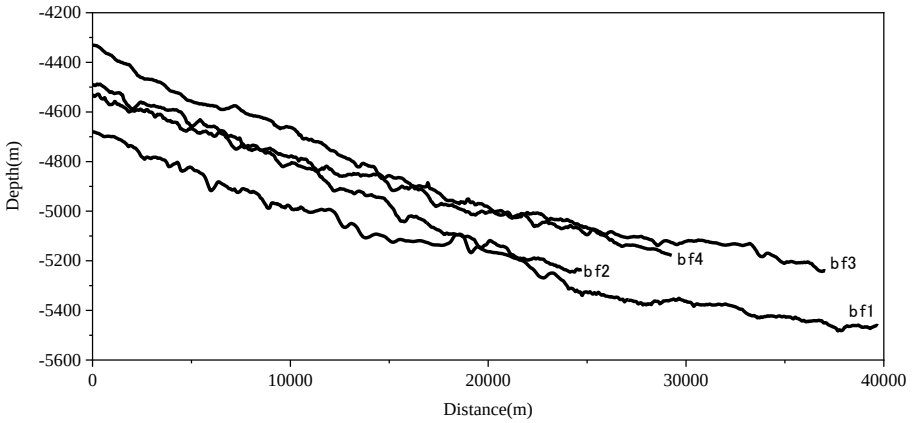

Figure S3. Sediment waves topography profile of Suda guyot.

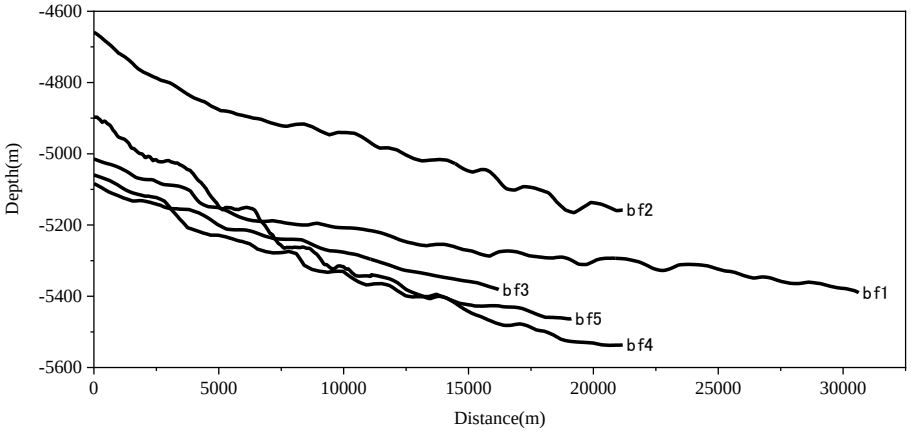

Figure S4. Sediment waves topography profile of Arnold guyot.

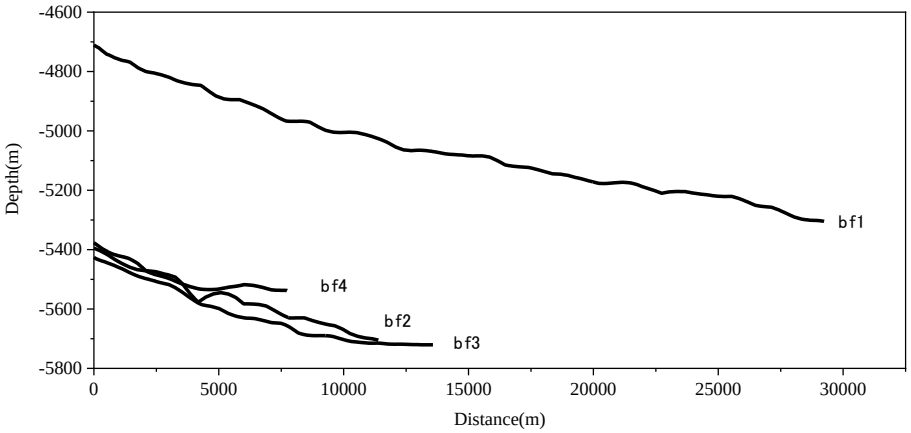

Figure S5. Sediment waves topography profile of Lamont guyot.

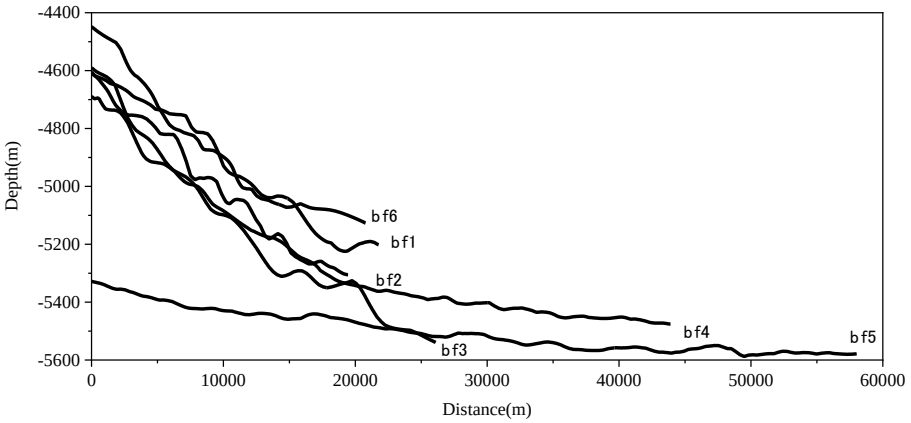

Figure S6. Sediment wave topography profile of Niulang and Zhinyv guyot.

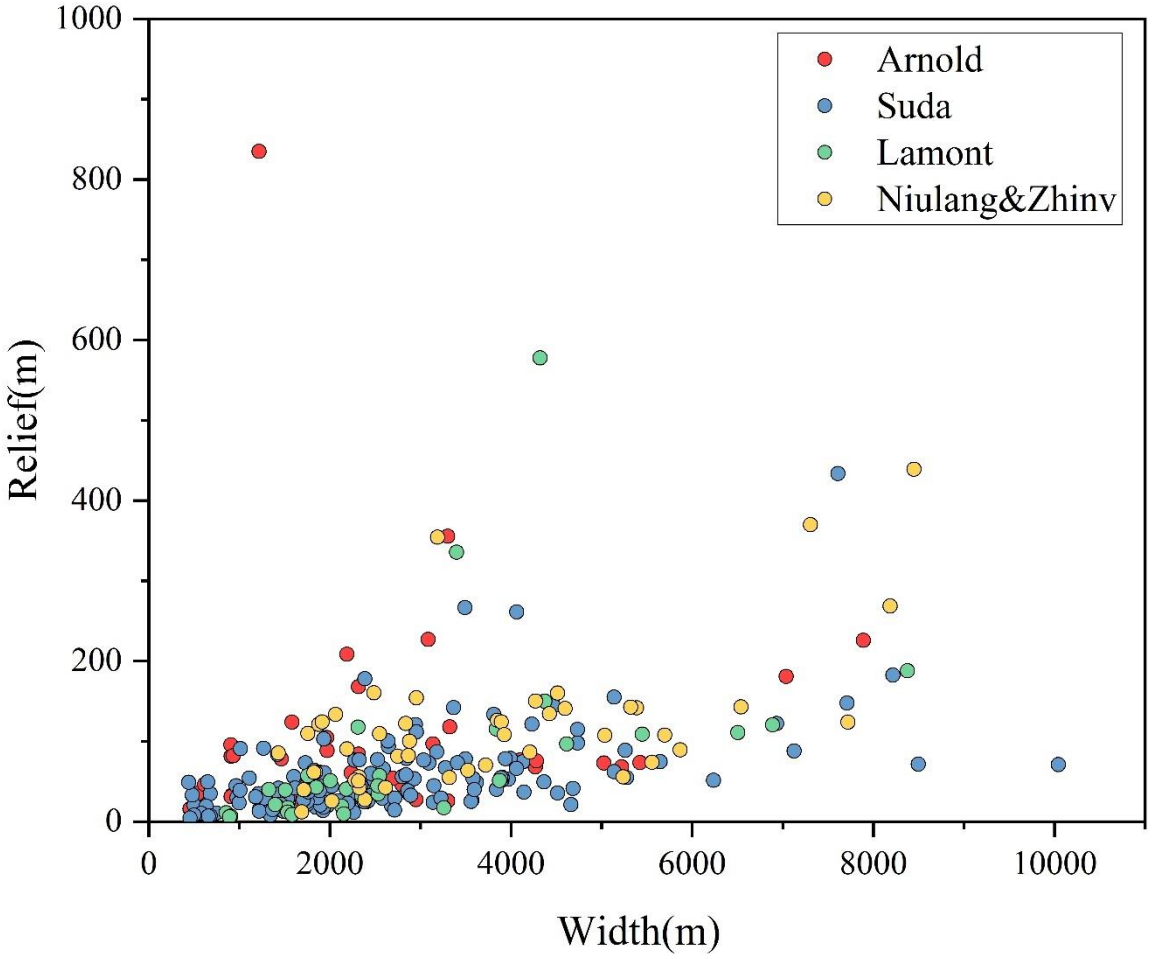

Figure S7. Relationship between the width and relief of gullies and channels.

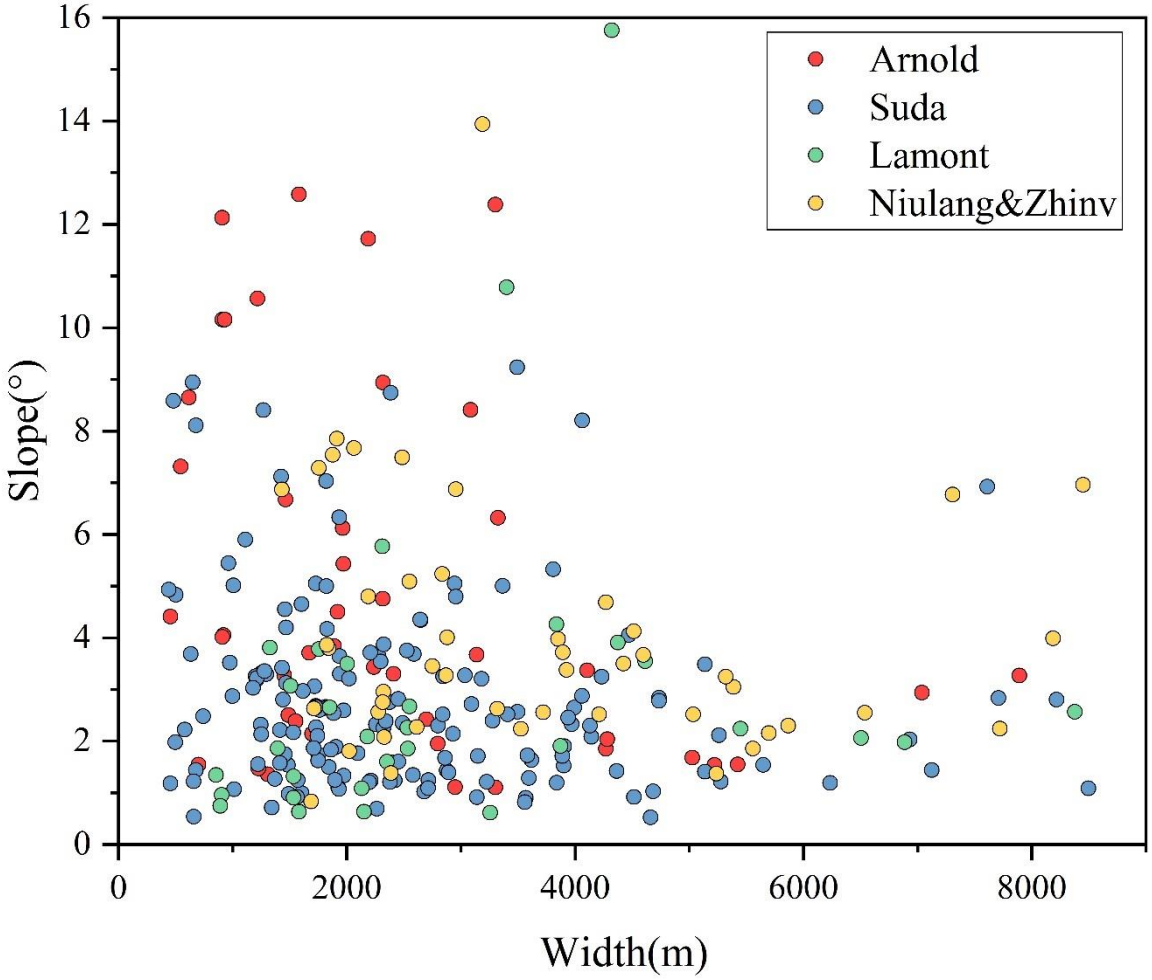

Figure S8. Relationship between the width and slope of gullies and channels.

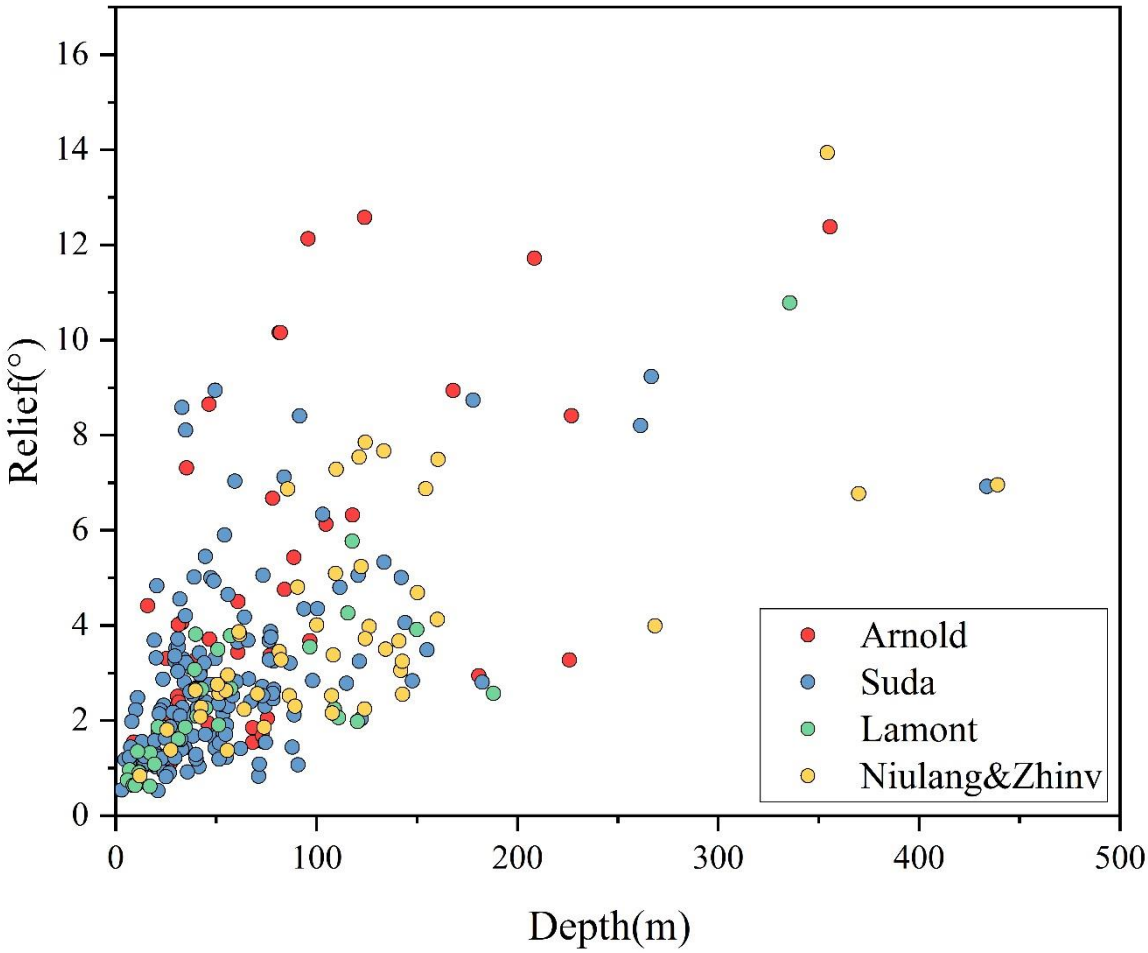

Figure S9. Relationship between the relief and slope of gullies and channels.

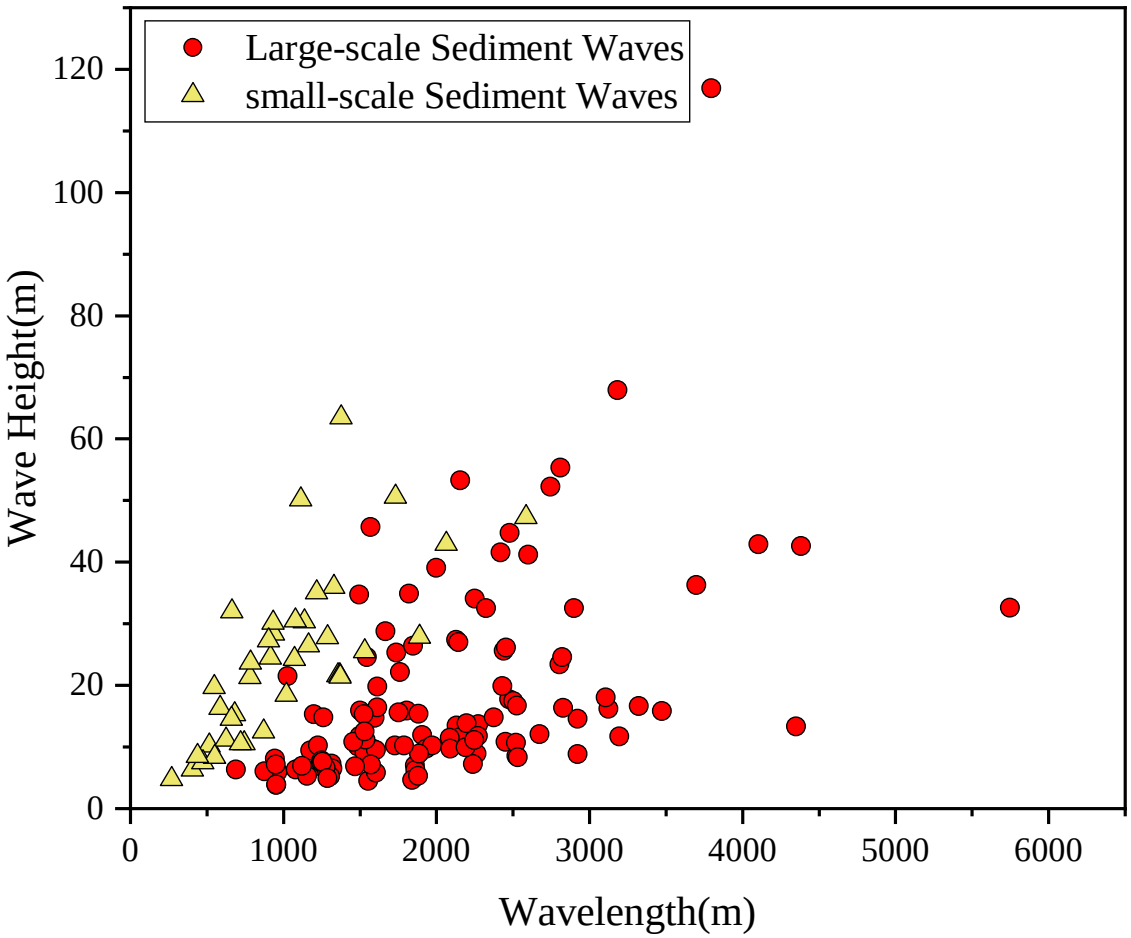

Figure S10. Relationship between the width and height of gullies and channels.

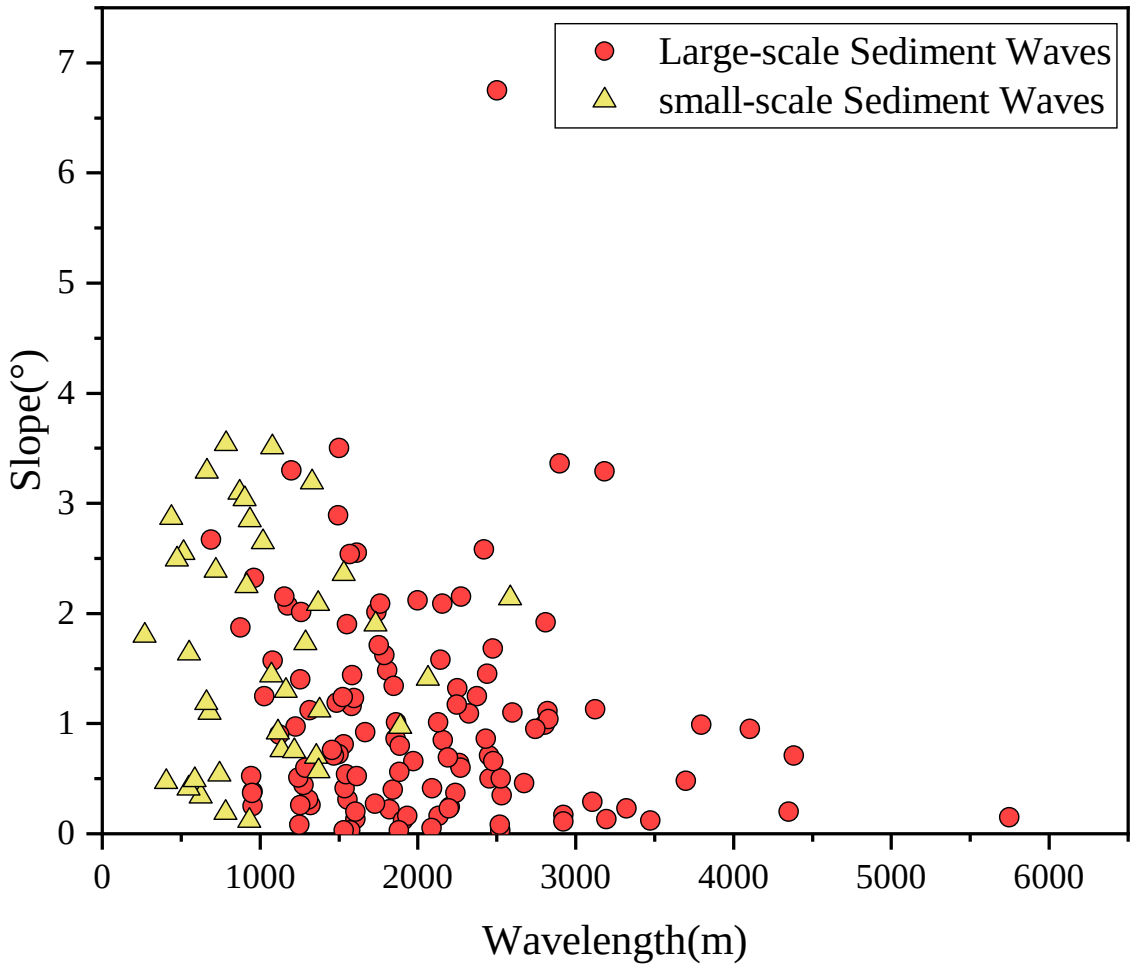

Figure S11. Relationship between the wavelength and slope of sediment waves at different scales.

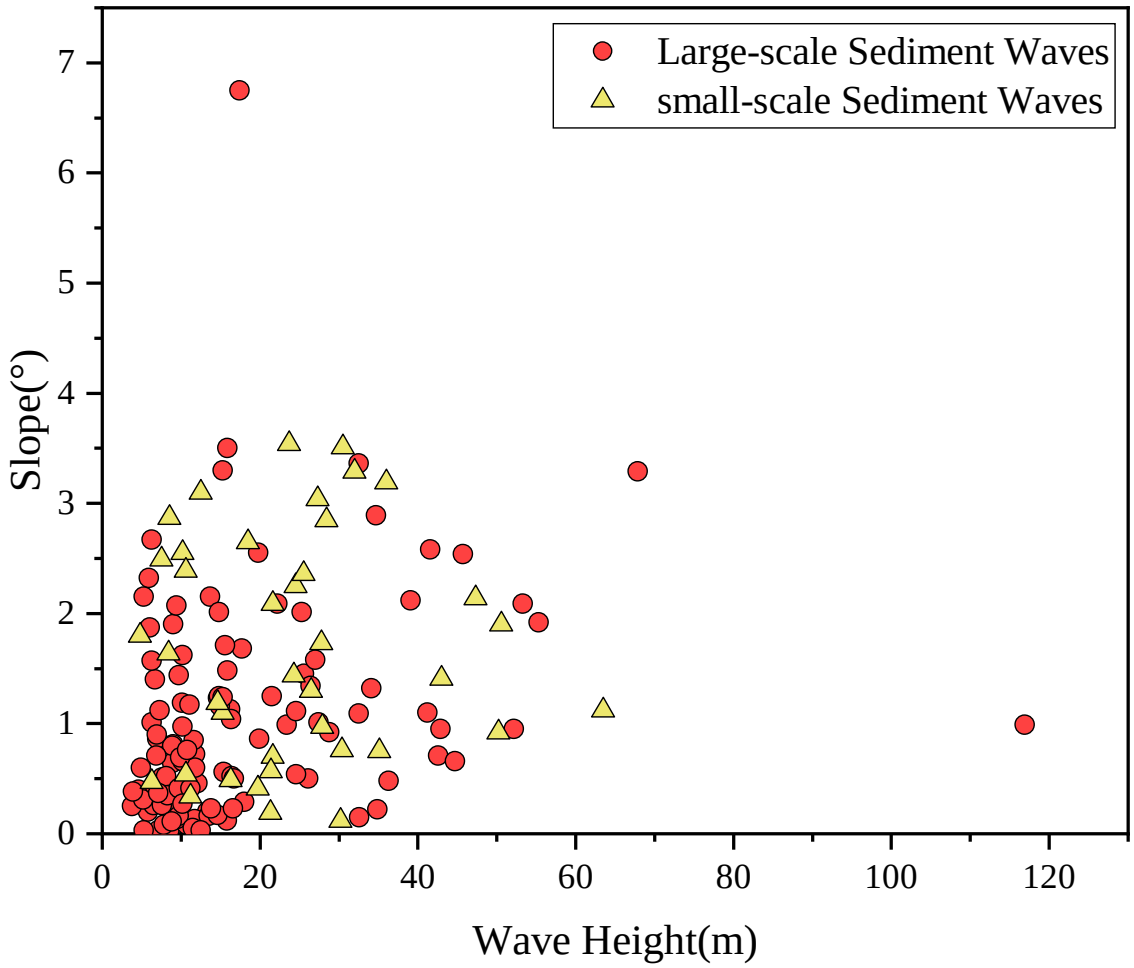

Figure S12. Relationship between the wave height and slope of sediment waves at different scales.

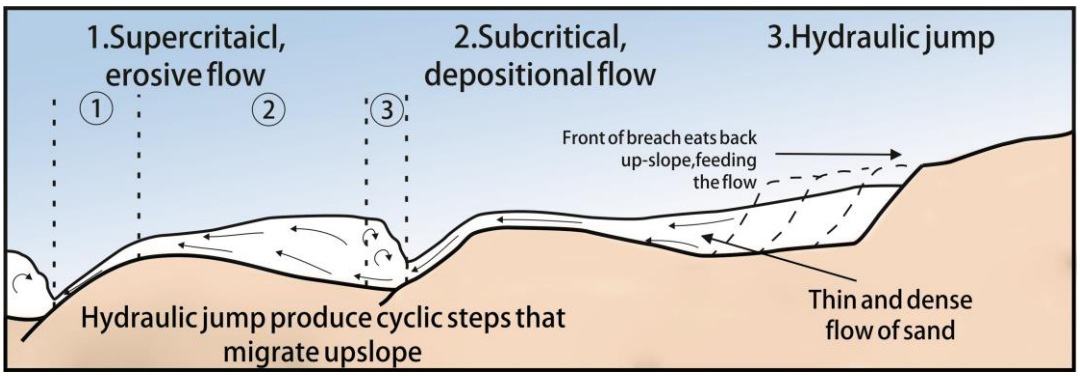

Figure S13. Small-scale sediment wave formation model (modified from Symons et al., 2016) [22].

Table S1. Aprons' topography data

	Number	Sediment and Debris Runout Distance (km)	Maximum Runout Distance (km)	Sediment and Debris Run from the Headwall Base (km)	Area of Apron Deposit (km²)	Scarp Shape	Scarp Length (km)	Fan Area (km²)	Type of Landslide	Slope (°)	Backscatter (dB)
Arnold	AP-01	51.00	51.00	30.00	439.32	Convex arc	6.8	1484.19	Slump	3	−24.0
	AP-02	51.84	51.85	28.87	770.51	Complex arc	31.1	1801.19	Debris avalanche	3	−28.5
	AP-03	49.86	51.62	10.71	449.05	Complex arc	14.3	1114.24	Rock failure	3	−33.0
	AP-04	54.58	54.58	22.63	988.43	Complex arc	41.7	2479.59	Debris avalanche	3	−34.0
	AP-05	20.25	27.12	8.74	41.64	Invagination arc	14.2	126.70	Debris avalanche	5	—
Lamont	AP-01	29.6.00	42.10	10.8.0	351.70	Complex arc	33.5	756.70	Debris avalanche	3	−35.0
	AP-02	35.4.00	39.80	16.7.0	255.20	Invagination arc	37.3	139.00	Debris avalanche	3	−35.0
	AP-03	32.00	32.00	9.65	169.90	Complex arc	32.4	605.80	Debris avalanche	5	−35.0
	AP-04	23.9.00	26.30	12.90	308.70	Complex arc	40.7	807.90	Rock failure	7	−35.0
	AP-05	24.4.00	28.90	5.80	364.00	Invagination arc	17.4	505.00	Debris avalanche	3	−31.0
	AP-06	33.4.00	39.30	13.90	442.10	Complex arc	47.8	941.80	Debris avalanche	1	−34.5
	AP-07	16.5.00	25.30	6.40	231.40	Complex arc	19.3	490.00	Debris avalanche	7	−33.5
	AP-08	26.7.00	26.70	20.80	28.40	Invagination arc	19.0	243.25	Debris avalanche	3	−34.5
Niulang and Zhinyv	AP-01	62.85	75.84	32.68	1432.21	Complex arc	35.6	3351.00	Debris avalanche	3	−36.0
	AP-02	24.18	24.18	19.40	98.91	Complex arc	17.2	504.00	Debris avalanche	5	—
	AP-03-e	54.62	54.62	44.81	502.56	Invagination arc	20.4	2204.00	Debris avalanche	3	−34.5
	AP-03-w	70.00	95.73	40.75	90.98						
	AP-04	24.91	29.25	11.15	193.85	Complex arc	18.9	364.00	Debris avalanche	5	−34.5
	AP-05	39.36	52.39	17.73	605.70	Complex arc	21.1	1268.00	Debris avalanche	5	−34.5
	AP-06	51.16	51.16	32.12	504.21	Invagination arc	34.6	875.78	Debris avalanche	5	—
	AP-07	51.23	70.17	15.58	1022.64	Convex arc	20.4	1886.00	Debris avalanche	3	−32.0
	AP-08	38.92	38.92	24.09	179.45	Invagination arc	42.6	711.00	Debris avalanche	5	—
	AP-09	25.48	25.48	8.61	119.66	Invagination arc	6.8	161.00	Debris avalanche	7	−30.5
	AP-010-s	70.37	70.37	37.01	650.53	Complex arc	20.4	2444.00	Debris avalanche	5	−34.5
	AP-010-n	39.22	39.22	16.87	376.75						
Suda	AP-01	120.52	120.52	31.69	8625.75	Complex arc	42.0	11661.00	Slump	1	−31.0
	AP-02	17.27	17.27	12.15	32.15	Invagination arc	6.5	125.50	Debris avalanche	2.5	−21.5
	AP-03	13.41	13.41	9.70	54.00	Invagination arc	13.5	106.10	Debris avalanche	7.5	−19.5
	AP-04	19.43	21.31	13.37	102.60	Invagination arc	11.6	234.70	Debris avalanche	5	−19.0
	AP-05	25.59	30.52	12.56	387.89	Complex arc	13.9	640.50	Rock failure	3	−21.5

Table S2. Sediment waves deposit' topography data

	Number of Profiles	Wavelength (m)	Wave Height (m)	Slope (°)	Depth Range (m)	Type of Cross-Section	Crest Pattern
Arnold	1	995–3145	4.3–22.4	0.1–1.9	5000–5400	Upslope asymmetric	Sinuous, straight
	2	1345–2337	9.7–31.5	0.77–1.43	4600–5200	Upslope asymmetric, symmetric	Crescentic, sinuous
	3	1507–4228	5.6–15.3	0.77–1.43	5000–5400	Symmetric	Straight, crescentic
	4	997–2783	4.8–75.9	0.64–2.92	4890–5600	Upslope asymmetric, symmetric	Reverse crescentic
	5	1520–2825	10.8–21.1	0.67–2.52	5000–5500	Symmetric	Sinuous
Lamont	1	963–3125	5.9–17.7	0.24–6.75	4700–5300	Symmetric	Sinuous
	2	876–2420	6.0–41.6	0.22–2.58	5400–5700	Symmetric	Sinuous
	3	1080–2441	6.3–25.6	0.64–2.15	5400–5700	Symmetric	Reverse crescentic
	4	690–1555	4.5–9.4	0.31–2.67	5400–5500	Symmetric	Crescentic
Niulang and Zhinyv	1	1009–2425	13.8–46.7	1.71–3.22	4600–5200	Symmetric	Sinuous
	2	1724–2885	26.5–63.8	1.46–3.56	4600–5300	Symmetric, upslope asymmetric	Sinuous
	3	2430–4486	15.1–85.2	0.60–3.84	4500–5500	Symmetric	Sinuous
	4	1716–3390	6.9–56.5	0.02–2.18	4900–5500	Symmetric	Reverse crescentic
	5	1301–4826	8.4–29.5	0.01–0.49	5300–5600	Symmetric	Crescentic, straight
	6	2510–3247	40.3–60.4	1.72–3.85	4750–5050	Symmetric	Sinuous
	2	1123–3183	6.9–67.9	0.52–3.29	5600–6000	Symmetric, upslope asymmetric	Straight
	3	1495–3796	11.8–116.9	0.6–2.89	5500–6100	Symmetric	Sinuous
	4	1029–2821	10.2–24.56	1.11–2.09	5600–5900	Symmetric	Reverse crescentic
	5	1879–4103	5.3–42.9	0.03–1.04	5200–5500	Symmetric	Reverse crescentic
	6	1288–3322	4.9–45.7	0.03–2.54	5300–5800	Symmetric	Reverse crescentic, straight
	7	2144–3699	27–53.3	0.48–2.09	5350–5800	Symmetric, upslope asymmetric	Reverse crescentic, straight
Suda	1	514–1732	10.2–63.4	0.7–3.19	4800–5500	Upslope asymmetric	Crescentic
	2	916–2586	24.5–47.3	0.75–2.36	4700–5200	Upslope asymmetric	Crescentic
	3	268–1890	4.8–30.2	0.12–3.04	4500–5200	Up, downslope asymmetric	Crescentic
	4	439–1371	8.4–32	0.41–3.54	4600–5200	Symmetric, upslope asymmetric	Crescentic